Rate constants for the collisional dissociation of N2O5 by N2

A. A. Viggiano, J. A. Davidson, F. C. Fehsenfeld, and E. E. Ferguson

Citation: The Journal of Chemical Physics **74**, 6113 (1981); doi: 10.1063/1.441055
View online: http://dx.doi.org/10.1063/1.441055
View Table of Contents: http://scitation.aip.org/content/aip/journal/jcp/74/11?ver=pdfcov
Published by the AIP Publishing

Rate constants for the collisional dissociation of N_2O_5 by N_2

A. A. Viggiano,[a] J. A. Davidson,[b] F. C. Fehsenfeld, and E. E. Ferguson[a]

Aeronomy Laboratory, NOAA Environmental Research Laboratories, Boulder, Colorado 80303
(Received 30 January 1979; accepted 13 January 1981)

The rate constants for the collisional dissociation of N_2O_5 by N_2 are measured over the pressure and temperature ranges of 10 to 800 Torr and 285 to 384 K, respectively. The measurements are carried out in flow-through reaction cells of different volumes, the N_2O_5 being detected by selected ion–molecule reactions in a flowing afterglow apparatus. The present rate constants are somewhat smaller than those of earlier studies and also suggest that the transition from second- to first-order kinetics occurs at lower pressures than was earlier thought. The data are fitted to theoretical models of varying sophistication. The recommended values for use in extrapolation for the limiting low-pressure and high-pressure rate constants corresponding to the first-order Troe extension of the Lindeman–Hinshelwood model for $F_{cent}^{SC} = 0.572$ are $k_0 = 1.15\times10^{-5}$ exp (− 19.70 kcal/mol/RT) $cm^3\,s^{-1}$ and $k_\infty = 1.21\times10^{17}$exp(− 25.41 kcal/mol/RT) s^{-1}. Other forms yield similar results.

INTRODUCTION

N_2O_5 is an important intermediary in the odd-nitrogen chemistry of the earth's atmosphere. It is formed by the association of NO_2 and NO_3

$$NO_2 + NO_3 + M \rightarrow N_2O_5 + M \quad (1)$$

and is destroyed by collisional dissociation

$$N_2O_5 + M \rightarrow NO_2 + NO_3 + M \quad (2)$$

as well as photodissociation and perhaps chemical reaction. The destruction processes are sufficiently slow in the stratosphere, however, that N_2O_5 can represent a significant reservoir for odd nitrogen.[1,2] It is important, therefore, to the understanding of the atmospheric chemistry to quantify the collisional association and dissociation rates of N_2O_5 over the range of atmospheric temperature, particularly those of the stratosphere, 200–300 K.

The collisional dissociation of N_2O_5 also represents a challenging test of the various theories that describe molecular dissociation. Accordingly, this process has been the subject of numerous previous experimental[3–14] and theoretical[15–21] studies.

Prior to this study the most extensive of the experimental investigations has been carried out by Mills and Johnston[5] and by Johnston and Perrine,[7] with the results subsequently reinterpreted by Johnston and White.[16] These measurements were carried out between 273 and 344 K in a variety of buffer gases and over a very wide pressure range, which encompassed the transition from second- to first-order kinetics that occurs with increasing pressure. However, the observed pressure dependence of the collisional dissociation rate constants through this transition was not in agreement with that predicted by RRKM theory.[20]

Recent studies[22] of thermal-energy positive and negative ion reactions with N_2O_5 have provided us with a new technique for investigating the neutral chemistry of N_2O_5, in which the detection of N_2O_5 is accomplished by chemical-ionization mass spectrometry. In the present study, the rate of collisional dissociation of N_2O_5 by N_2 has been measured between 285 and 384 K and a pressure range of 10 to 800 Torr. The present rates are lower than those obtained in the 1950's, and predict a transition from second- to first-order kinetics that is in much better agreement with RRKM theory.

While these experiments were in progress, Connell and Johnston[13] completed a set of experiments pertinent to this reaction. Their measurements covered a large pressure range at temperatures from 262 to 307 K. At low pressures their results agreed with the experimental results obtained in the 1950's but indicated the change-over from second- to first-order kinetics to occur at lower pressures than the old results.

While the temperature and pressure range of the present data infrequently overlap the data of Connell and Johnston our results appear to be somewhat lower than those of Connell and Johnston even considering the combined uncertainty of the two measurement sets. However, the dependency of the rate constant on pressure (the falloff curve) and temperature (Arrhenius plots) reported here agree quite well with the Connell and Johnston results.

EXPERIMENTAL TECHNIQUE

General description

Figure 1 shows a schematic representation of the apparatus used in these measurements. A sample of N_2O_5 is contained in a flow through vessel. The N_2O_5 is prepared through the oxidation of NO by O_3 as described earlier.[22] In the N_2O_5 sample the impurity level of NO_2 is $<1\%$ as determined by laser magnetic resonance[23] and the HNO_3 impurity level is $<5\%$ determined by Cl^- chemical ionization.[22]

A nitrogen carrier gas flow of a few STP $cm^3\,s^{-1}$, trapped to remove H_2O and, hence, prevent the heterogeneous conversion of N_2O_5 to HNO_3,[24] enters the vessel containing N_2O_5 held at − 50 C by an acetonitrile and dry-ice slush bath as measured by a chromel–alumel

[a] Also affiliated with the Department of Chemistry, University of Colorado, Boulder.

[b] Present address: Wittenberg University, Springfield, Ohio 05401.

 0021-9606/81/116113-13$01.00

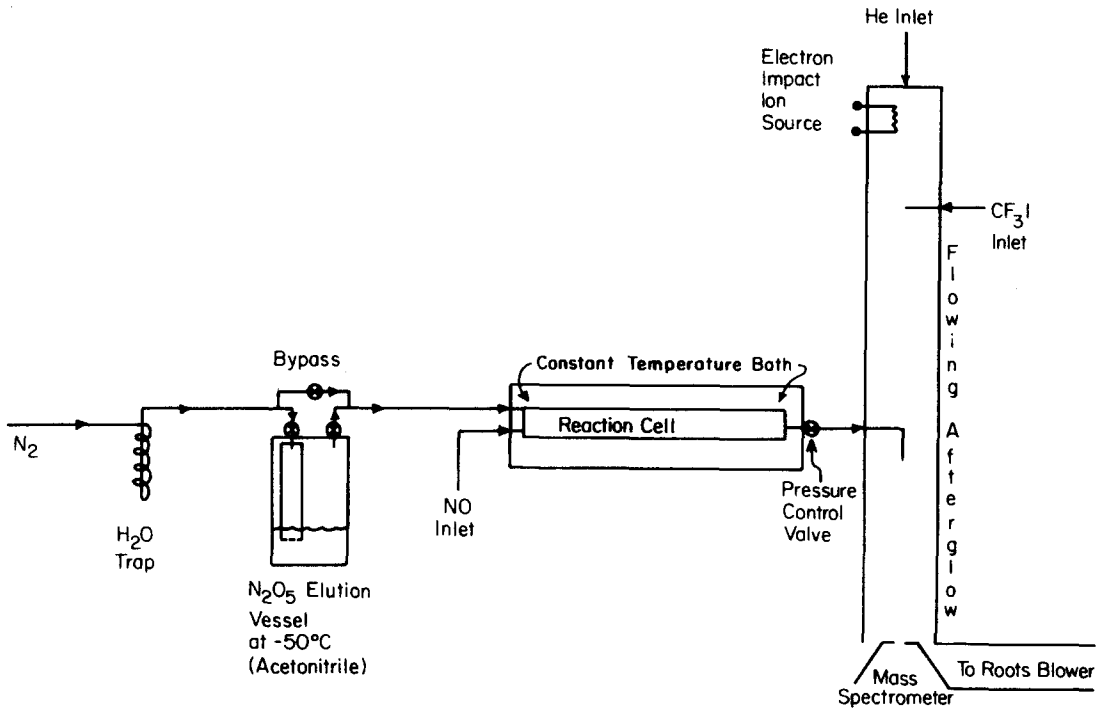

FIG. 1. Schematic representation of the N_2O_5 collisional dissociation apparatus and flowing afterglow chemical ionization detector.

thermocouple accurate to 0.1 °C. This temperature is held constant to a few tenths of a °C during the course of an experiment. On exiting the vessel the nitrogen carrier contains $\leq 2\%$ N_2O_5. The N_2 containing N_2O_5 proceeds to the reaction cell.

The mixture of N_2O_5 in N_2 then enters the reaction cell and mixes with a flow of NO, a few percent as large as the N_2 flow. The NO is added in sufficient quantity to scavenge all the NO_3 dissociation product via the fast reaction[4]

$$NO + NO_3 \rightarrow 2NO_2 , \quad (3)$$

thereby preventing the NO_2 and NO_3 products from recombining.

In order to verify that the scavenging reaction is much faster than the recombination reaction, the I^- and NO_3^- ion signals are measured as a function of NO flow. A large change in the ion signals is observed upon addition of the smallest controllable NO flow (3×10^{-3} STP $cm^3\,s^{-1}$); no further change is noticed upon further addition of NO. Ten times this minimum flow is used in these experiments.

Upon leaving the reaction cell the N_2O_5, NO, NO_2, and N_2 flow into a room temperature flowing afterglow apparatus used as a chemical ionization mass spectrometer to detect N_2O_5. The reaction of N_2O_5 with I^-

$$I^- + N_2O_5 \rightarrow NO_3^- + INO_2 \quad (4)$$

proved to be the most suitable reaction, since Reaction (4) is fast[22] and I^- does not react with NO, N_2, NO_2,[25] or HNO_3.[26]

The flowing afterglow is described in detail elsewhere.[27] Briefly, a helium carrier gas flow of 160 STP $cm^3\,s^{-1}$ is used. The carrier is ionized by an electron impact ion source. The secondary electrons produced by the ionization are subsequently attached by CF_3I to produce I^-. All other negative ion abundances are $\leq 2\%$ of that of I^-. The helium buffer then carries the I^- ions downstream where the gases from the thermal decomposition reaction cell are added. After a reaction region the ions are mass analyzed and detected by a quadrupole mass spectrometer.

Fixed length reaction cells

In order to study the reaction over a wide temperature and pressure range three fixed length Pyrex tubes cleaned with HF are used. A tube with a radius of 9.5 mm and a volume of 138 cm^3 is used for pressures ≤ 100 Torr and is referred to as cell 1. For pressures ≥ 100 Torr two cells, referred to as cell 2 and cell 3, having radii of 3.5 and 5.0 mm and volumes of 43 and 200 cm^3, respectively, are used. Cell 1 is a straight tube while cells 2 and 3 are wound into coils of 7 cm radii to fit into space requirements. The use of three cells allows elimination of errors due to radial and axial diffusion from the measurements as explained in detail by Viggiano.[28]

The experimental apparatus for these cells is shown in Fig. 2. The N_2/N_2O_5 gas mixture and the NO scavenger gas enter the flow reactor through separate capillaries, where the gases are preheated before mixing. The NO, N_2O_5, and N_2 then enter the reaction cell. Within a few percent of the total reaction length the gases are completely mixed and fully developed, incompressable, nonturbulent, viscous flow is established.[29] Pressure is maintained by a valve at the end of the cell. Pressure remains constant to $\leq 1\%$ during an experiment as measured at the center of the reaction cell by a capacitance manometer accurate to $\leq 1\%$ over the entire range

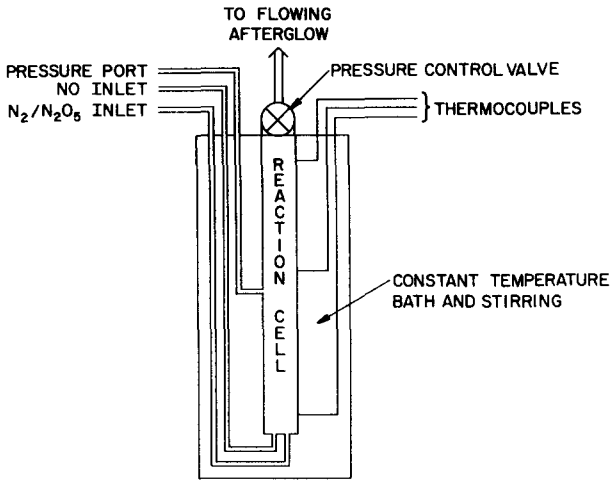

FIG. 2. Schematic representation of the fixed length reaction cells.

of pressures. The gases upon leaving the reaction cell pass into the flowing afterglow detector.

Each cell is immersed in a variable-temperature bath. Insulation and stirring keep temperature gradients $\leq 0.4\,^{\circ}C$ as measured by three chromel–alumel thermocouples placed at various heights in the bath. An oil bath is used for runs taken in cells 1 and 2 and 2-propanol is used for experiments in cell 3 (lower temperatures). The baths are warmed by resistance heaters and are cooled by a copper heat exchange coil, through which 6 °C tap water or liquid nitrogen is circulated.

Initially the I^- and NO_3^- signals are recorded when the bath temperature is sufficiently low that no detectable amount of N_2O_5 is dissociated during passage through the cell. Subsequently, the ion signals are recorded as the temperature of the reaction cell is raised in increments of 3 to 5 °C resulting in a progressive reduction of N_2O_5 leaving the reaction cell. Finally, a temperature is reached at which no detectable N_2O_5 survives the reaction cell. In addition, data is acquired starting at a high temperature where no detectable N_2O_5 is present and progressively cooling the cell until no N_2O_5 is decomposed in the cell.

For runs taken while decreasing the temperature a check is made on the ion signal stability at the end of the run. The N_2O_5 is removed from the N_2 by bypassing the N_2O_5 elution vessel. In this way the ion signals obtained in the absence of N_2O_5 at the beginning and end of the run are compared. The signals agree within a few percent.

Variable length reaction cell

A variable length cell is used to broaden the pressure range of data and also serves as a check on the fixed length tube measurements. The apparatus for the variable length cell is shown in Fig. 3. The N_2/N_2O_5 mixture is added through a movable inlet into a 8.2 mm radius Pyrex tube one meter long. The NO is added upstream of the N_2O_5 injector. A second N_2 flow, approximately the same magnitude as the N_2O_5 saturated N_2, is added upstream in order to prevent a region of stagnated flow upstream of the movable inlet. The operating pressure and residence time of the N_2O_5 in the cell is controlled by the valve which separates the flow cell from the flowing afterglow. Temperature in the variable length cell is maintained by a heating fluid which circulates through a jacket concentric to the flow tube. Water and dibutyl-phthalate are used as the heating fluid. In this manner, temperature is regulated to better than 0.5 °C.

Data is acquired by monitoring the I^- ion signal as a function of the inlet position. This inlet is moved from 8 to 74 cm from the end of the temperature jacket. The I^- signal in the absence of N_2O_5 is obtained by bypassing the N_2O_5 elution vessel.

DATA ANALYSIS AND RESULTS

The thermal decomposition rate constant $k_1(T, N_2)$ (1 refers to first-order rate) in the fixed length cells is given by

$$k_1 + 1/\tau \ln([N_2O_5]_0/[N_2O_5]_T)\,, \tag{5}$$

where τ is the mean residence time of the N_2O_5 in the reaction cell and is determined from the cell volume and the total flow rate, $[N_2O_5]_0$ is the N_2O_5 number density in the reaction cell when no decomposition occurs, and $[N_2O_5]_T$ is the N_2O_5 number density remaining after dissociation on passage through the reaction cell at the temperature T. The number densities $[N_2O_5]_0$ and $[N_2O_5]_T$ are not measured directly but rather the ratio needed in Eq. (5) is related to I^- signals measured in the flowing afterglow apparatus in the manner described below.

In the flowing afterglow detector in N_2O_5 concentration is related to the monitor ion number density I^- by

$$\ln([I^-]_c/[I^-]) = k_4[N_2O_5]\,t\,, \tag{6}$$

where $[I^-]_c$ is the iodide ion number density with no N_2O_5 entering the flowing afterglow (i.e., complete dissociation or the bypass open), I^- is the number density corresponding to a nonzero N_2O_5 concentration, $[N_2O_5]$, k_4 is the rate constant for the monitor reaction (4), and t is the reaction time in the flowing afterglow.

The N_2O_5 concentration in Eq. (6) is the number density of N_2O_5 in the flowing afterglow. However, this concentration is directly proportional to the number

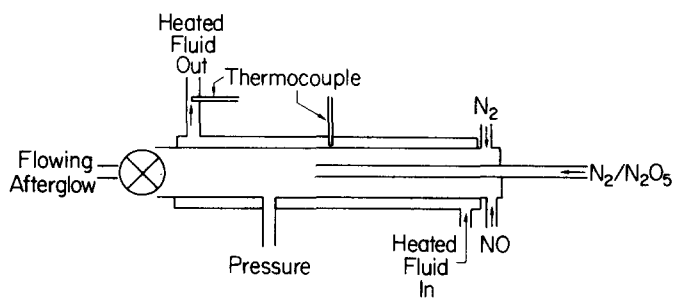

FIG. 3. Schematic representation of the variable length reaction cells.

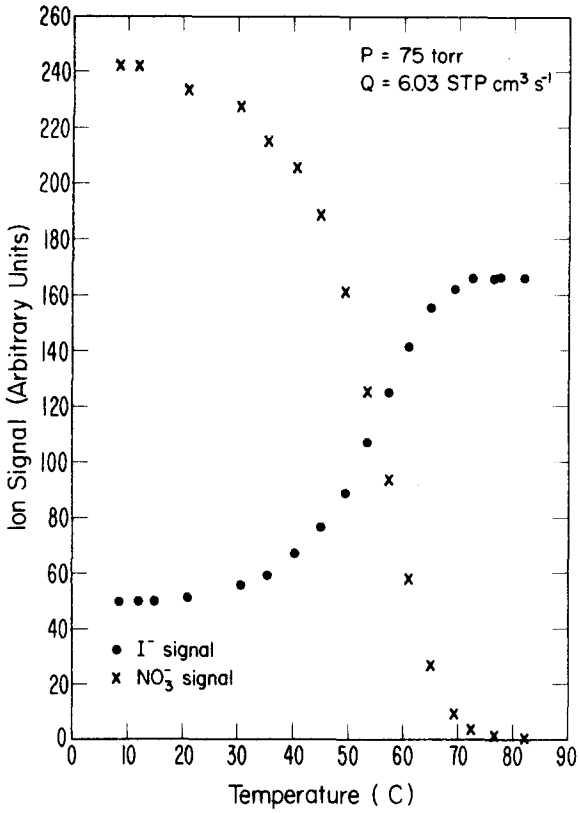

FIG. 4. I^- and NO_3^- ion signals taken in cell 1 as a function of temperature.

density at the exit of the thermal decomposition cells, which is the concentration needed in Eq. (5). Equation (6) can be written for two reaction cell temperatures, a low temperature where no N_2O_5 dissociation occurs and a higher temperature where some dissociation occurs in the reaction cell. Upon division, these two equations relate the N_2O_5 concentration at the exit of the reaction cell to the concentration in the flowing afterglow by

$$\ln([I^-]_c/[I^-]_0)/\ln([I^-]_c/[I^-]_T)=[N_2O_5]_0/[N_2O_5]_T\ , \qquad (7)$$

where $[I^-]_0$ is the iodide number density corresponding to no N_2O_5 dissociation, $[I^-]_T$ is the iodide number density corresponding to partial dissociation in the reaction cell at a temperature T, and the right-hand side of this reaction is the ratio of N_2O_5 densities needed in Eq. (5). It is worth noting that the rate constant k_4 for loss of I^- by reaction with N_2O_5 cancels out of the analysis. Therefore, the uncertainties in the measurement of k_4 do not influence the determination of k_1 in the present experiment.

Data analysis in the variable length cell is quite similar. The principal difference involves the substitution of distance for time in Eq. (5), where the two quantities are related by the average velocity in the tube. Upon this substitution one obtains

$$k_1=\bar{v}/\Delta Z\ln(\ln([I^-]_c/[I^-]_0/\ln([I^-]_c/[I^-]_z))\ , \qquad (8)$$

where $\bar{v}$ is the average velocity in the tube, z is the reaction length, $[I^-]_c$ is the I^- signal when the N_2 passes the N_2O_5 vessel, $[I^-]_0$ is the I^- signal with the injector at the minimum reactor distance, and $[I^-]_z$ is the I^- signal as a function of distance.

An example of data reduction in the fixed length cells is shown in Fig. 4, where the primary I^- ion signal and the product NO_3^- ion signal are plotted as a function of temperature from 281 to 355 K. These data have been taken in reaction cell 1 at a pressure of 75 Torr. The nitrogen flow in this measurement is 6.00 STP $cm^3\,s^{-1}$ and the NO flow 3.0×10^{-2} STP $cm^3\,s^{-1}$. At temperatures below 285 K the monitor ion signals do not change indicating no detectable N_2O_5 dissociation occurs below this temperature. In this manner, $[I^-]_0$ is established for this run of data. In Fig. 4 one can see that as the temperature is increased, the I^- signal increases and the NO_3^- signal decreases, reflecting the loss of N_2O_5 by dissociation. This establishes a series of $[I^-]_T$ values at intermediate temperatures. Finally, at temperatures above 350 K, the I^- signal is independent of temperature, with the NO_3^- signal equal to zero, indicating that the dissociation of N_2O_5 is complete, thereby establishing $[I^-]_c$. As can easily be seen in Fig. 4 the increase in the I^- signal does not balance the decrease in the NO_3^- signal due to mass discrimination in the quadrupole mass filter. This discrimination does not enter into our calculations. Values of $[I^-]_T$ too close to either end point are not used in determining a rate constant, since the error in determining k_1 increases as the difference between $[I^-]_c$ or $[I^-]_0$ and $[I^-]_T$ becomes small. Similar measurement sequences are repeated at other pressures and cell sizes. As a check for systematic error data is taken while both increasing and decreasing the temperature and no appreciable difference in the determination of k_1 is found.

The rate constants determined from the run of data shown in Fig. 4 are plotted in Arrhenius form in Fig. 5. The large dependence of k_1 on temperature is easily seen in Fig. 5, as k_1 increases 50 times as the temperature is raised approximately 40 K. The activation energy for this run of data is 21.1 kcal/mol.

Although this technique is direct and straightforward, it requires a high degree of ion-signal stability for the duration of time needed to change the cell temperature from the zero-dissociation limit to the complete-dissociation limit, typically on the order of one-half hour. Runs in which the ion signals vary by more than a few percent between the beginning and the end of the measurement are rejected.

Each parameter in the present experiments is measured with an accuracy of a few percent. The results are most sensitive to the measurement of $[I^-]_0$ where at temperatures approaching the point where no N_2O_5 is dissociated in the cell an error of a few percent can lead to a significant error of 10–20% in the calculated rate constant. To minimize this effect, k_1 is determined under circumstances where $[I^-]_T \leq 0.9\,I_0^-$. In addition, at least four sets of data are taken at each pressure in each cell to check for possible discrepancies in the rate constants. Consideration of these uncertainties as well as possible systematic errors in the determination of flow rate, pressure, cell volume,

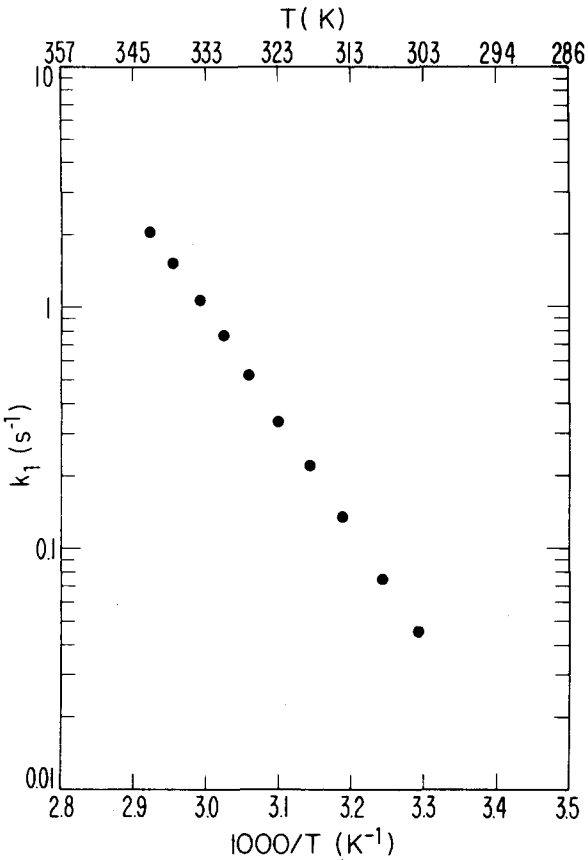

FIG. 5. Arrhenius plot of the rate constants obtained from the data shown in Fig. 4.

ion signals, and temperature lead to an estimated uncertainty of 40% in the rate constants here. Repeatability tests indicate that the random error is about one-half this value.

Referring to Eq. (8) one can see that a plot of $\ln\ln([I^-]_c/[I^-]_2)$ should be a straight line for data taken in the variable length cell. A typical plot is shown in Fig. 6. The data are taken at a temperature of 85.3 °C and a pressure of 10.3 Torr. The injector is moved from 8 cm from the end of the tube (4 cm on the plot) to 43 cm and back again. The rate constant for this run of data is 2.79 s^{-1}. Error estimates of this reactor are similar to those of the fixed length cells.

In any closed reactor, wall reactions can pose a serious problem. In these experiments N_2O_5 can undergo two types of loss on the wall. Conversion of N_2O_5 to HNO_3 on the wall

$$N_2O_5 + H_2O \xrightarrow{\text{wall}} 2HNO_3 \qquad (9)$$

is a well-known process.[24] Also, the wall can act as a dissociator to produce NO_2 and NO_3.

In the variable length cell wall conversion of N_2O_5 to HNO_3 can be easily checked. This is accomplished by taking data in the normal manner, with the exclusion of NO. In the absence of NO all the N_2O_5 dissociated reforms, since the equilibrium constant for Reactions (1) and (2) strongly favors N_2O_5 under the experimental conditions in these measurements, but any conversion to HNO_3 is irreversible. Data without NO is analyzed by Eq. (8) and the wall conversion reaction rate is subtracted from the total rate constant. For the run shown in Fig. 6 the measured wall conversion rate is $\leq 0.07\ s^{-1}$ which is less than 3% of the dissociation rate.

It is much harder to check for wall decomposition since the products reform in the absence of NO. One possible check is changing the surface to volume ratio of the reaction cells and looking for differences in the measured rate constants. At 100 Torr a comparison of this type can be made in cells 1 and 2 whose surface to volume ratio differ by almost a factor of 3. This comparison is shown in an Arrhenius plot in Fig. 7. Only a portion of the data from each cell is plotted to avoid overcrowding. Cell 1 data are represented by circles and triangles represent data from cell 2. No large discrepancies are evident.

One last test is made to check for wall reactions in cell 2. Just as in the variable length cell, NO is left out of the reaction cell. This time the only way to check for wall reaction is to heat the cell to higher temperatures than is normally done. At higher temperatures N_2O_5 is destroyed by a variety of possible processes. These include conversion of N_2O_5 to HNO_3 via Reaction (9), NO_3 destruction on the wall,

$$NO_3 \xrightarrow{\text{wall}} \text{products}\ , \qquad (10)$$

production of NO by some unknown mechanism, the self-reaction of NO_3

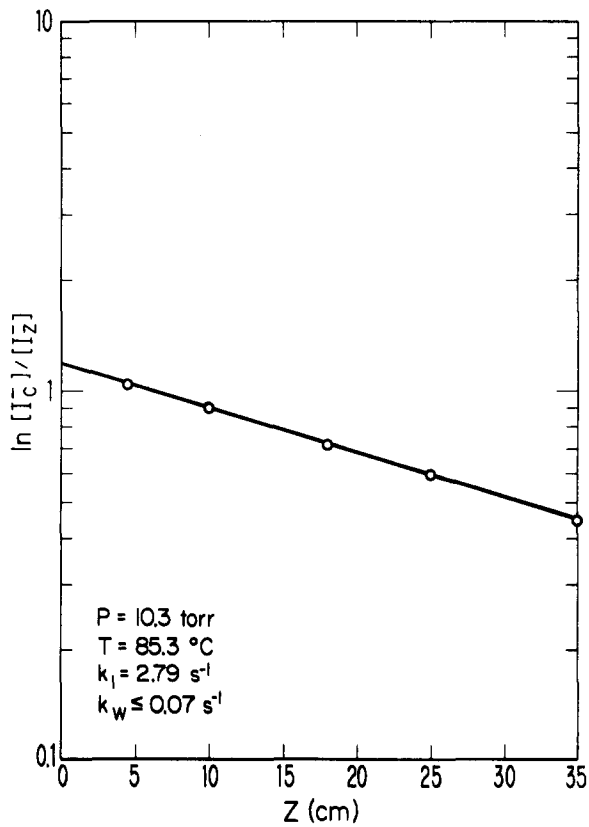

FIG. 6. Plot of $\ln\ln[I^-]_c/[I^-]_z$ vs z taken in the variable length cell.

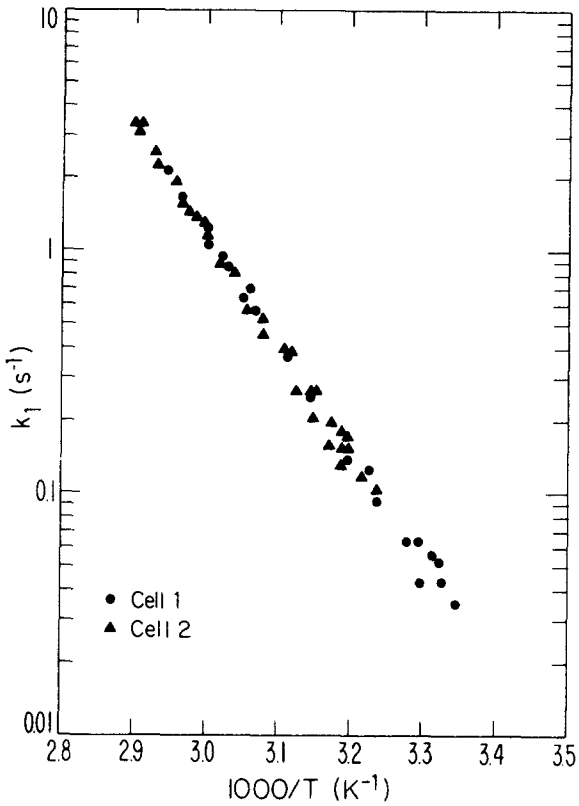

FIG. 7. Comparison of rate constants obtained in cell 1 and cell 2 at 100 Torr plotted in Arrhenius form.

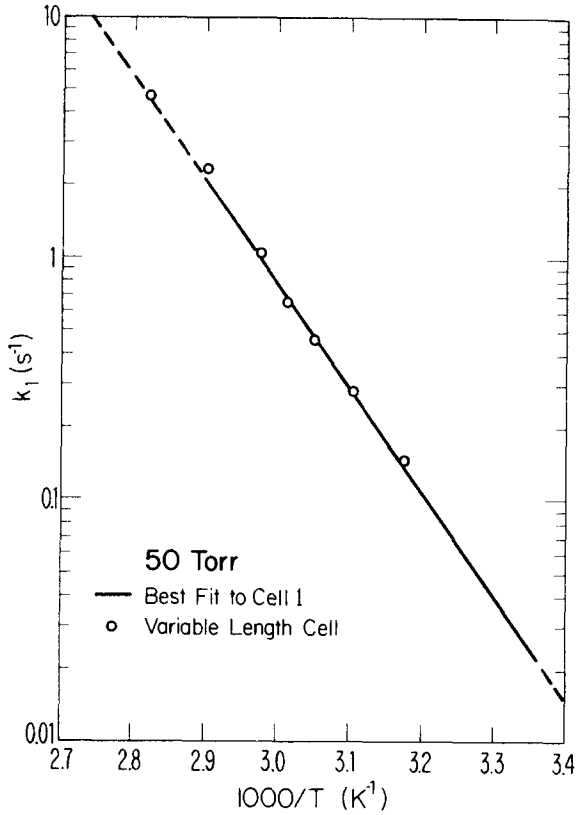

FIG. 9. Comparison of rate constants obtained in cell 1 at 50 Torr with those obtained in the variable length cell.

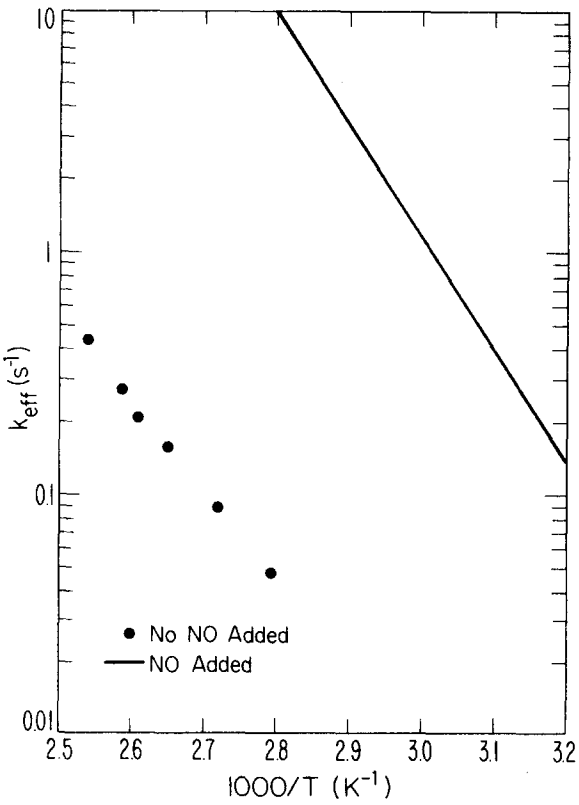

FIG. 8. Comparison of the rate constants obtained in cell 2 at 100 Torr with and without NO added.

$$NO_3 + NO_3 \rightarrow 2NO_2 + O_2 \ , \tag{11}$$

and finally a binary reaction of NO_2 and NO_3

$$NO_2 + NO_3 \rightarrow NO + O_2 + NO_2 \ . \tag{12}$$

Details of the mechanism for the thermal decomposition of N_2O_5 in the absence of NO are given by Johnston.[30]

If the data obtained in this manner is analyzed in the usual way, much smaller rate constants are obtained. Such results obtained without the NO scavenger are compared in Fig. 8 to those taken with NO. The solid line represents data taken with NO and the points are data taken without NO. The total destruction rate in the absence of NO, including wall conversion, is less than 1% of those with NO added and one can assume that wall conversion of N_2O_5 to HNO_3 is not a problem in this cell.

Figure 9 shows a comparison of data taken in the two types of reactors at 50 Torr. The line represents the data taken in cell 1 and the points are from the variable length cell. The agreement is excellent. No wall reactions are observed in the variable length cell at this pressure.

However, the good agreement noted at 50 Torr is absent when data from the same two cells are compared at 10 Torr, as shown in Fig. 10. A rather large discrepancy is seen at low temperatures or more precisely low rate constant. The effect is presumably due to the conversion of N_2O_5 to HNO_3 on the wall in cell 1. At this pressure wall conversion reactions correponding to 10% or less of k_1 are observed in the variable length

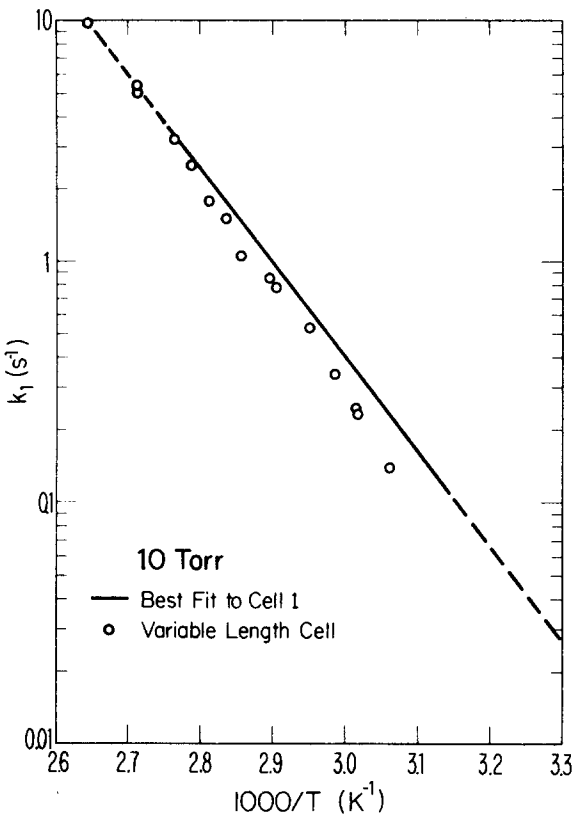

FIG. 10. Comparison of rate constants obtained in cell 1 at 100 Torr with those obtained in the variable length cell.

cell. It is therefore reasonable to expect that wall reactions of similar magnitude occur in cell 1.

The data at 30 Torr have a much smaller deviation than the deviation seen at 10 Torr. Since wall effects can only be accurately estimated in the variable length cell, data taken in this cell are used exclusively in the data base for pressures of 10 and 30 Torr to avoid errors due to HNO_3 conversion. Even in the variable length cell at pressures below 10 Torr the wall conversion rate is a large percentage of the total destruction rate. The magnitude of this effect is hard to estimate at low pressure and no data are included at pressures below 10 Torr.

DISCUSSION

In this manner N_2O_5 dissociation rates are determined over a temperature range of 285–384 K and a pressure range of 10–800 Torr. The results of these measurements are listed in Table I according to reaction cell along with the temperature (K) and N_2 number density (molecules cm^{-3}).

The data obtained at each pressure are combined and fit to an Arrhenius expression $k = A\exp(-E/RT)$, by a nonlinear least squares fit.[31] Equal percentage weights are used in accordance with our estimates of error. The results of these fits are listed in Table II along with the 95% confidence error limits on the activation energies E for statistical error only. Corresponding error limits for the pre-exponential factors A are not independently given since the two quantities are very highly correlated. Disregarding slight deviations due to measurement errors, a noticeable trend toward higher activation energies at higher pressures can be seen, as expected from unimolecular reaction theory.

The kinetic theory of the thermal decomposition of N_2O_5 has been discussed in detail.[15–21] The most rigorous theoretical treatment would involve a complete RRKM calculation or equivalent. Our present requirements are better served, however, by utilizing the simpler kinetic theory approximations which provide analytic expressions which predict the behavior of Reaction (2) in the transition region. By fitting these expressions to the present data one obtains both reasonability checks for the present results as well as providing a means for extrapolating our data for comparison with other experimental data or for use in atmospheric models. We have fit the present data to two such analytic expressions.

The simplest theoretical mechanism for Reaction (2) is due to Lindemann and Hinshelwood[32] which is written for N_2O_5 as

$$N_2O_5 + M \underset{k_f}{\overset{k_f}{\rightleftharpoons}} N_2O_5^* + M \,, \tag{13}$$

$$N_2O_5^* \xrightarrow{k_{uni}} NO_2 + NO_3 \,. \tag{14}$$

This representation uses a single rate constant to describe the behavior of all the states of N_2O_5 and a single activated complex $N_2O_5^*$ to describe Reaction (2) over the entire temperature and pressure range of interest.

The first-order rate constant for destruction of N_2O_5 based on this mechanism under steady state conditions is

$$k_1 = k_f k_{uni}[M]/(k_{uni} + k_r[M]) \,, \tag{15}$$

which can be rearranged as

$$k_1^{LH} = k_0[M]/(1 + k_0[M]/k_\infty) \,, \tag{16}$$

where k_0 and k_∞ are the second-order low pressure and first-order high pressure limits of the expression, respectively.

Johnston and White[16] have given a better expression for use in fitting data through the falloff region. They start with a general Lindeman–Hinshelwood formulation where Reactions (13) and (14) are written for each excited state of N_2O_5. Following a series of mathematical manipulations and the assumption that all collisions of excited states with the buffer result in deactivation (strong collision assumption), they obtain

$$J = \left(\frac{k_\infty - k}{k}\right)\left(\frac{k_0 - k_1}{k_1}\right) \;; \quad k_1 = k/[M] \,, \tag{17}$$

where J may be interpreted as the product of the average microscopic rate constants for decomposition from excited states and the average molecular state lifetime. Solving for reciprocal rate constant yields

$$2/k = \frac{1}{k_0 M} + \frac{1}{k_{00}} + \left(\frac{1}{k_0 M} + \frac{1}{k_\infty}\right)^2 + \frac{4(J-1)^{1/2}}{k_\infty k_0 M} \tag{18}$$

which reduces to Eq. (16) for $J = 1$. They have shown

TABLE I. Measured rate constants k_1 (s^{-1}) for the collisional dissociation of N_2O_5 by N_2 at various temperatures T (K) and number densities N_2 (molecule cm^{-3}).

Cell 1

T	N_2	k_1
330.2	1.49E+18	7.50E-01
324.2	1.52E+18	4.08E-01
320.9	1.54E+18	2.87E-01
316.6	1.56E+18	1.85E-01
312.8	1.58E+18	1.31E-01
309.7	1.59E+18	9.27E-02
305.6	1.61E+18	6.15E-02
300.8	1.64E+18	3.55E-02
296.5	1.66E+18	1.88E-02
335.0	1.44E+18	9.14E-01
328.9	1.47E+18	4.88E-01
324.0	1.49E+18	3.03E-01
319.2	1.51E+18	1.76E-01
313.9	1.54E+18	1.02E-01
310.6	1.56E+18	6.87E-02
306.9	1.58E+18	4.45E-02
301.3	1.60E+18	2.91E-02
336.0	1.50E+18	8.43E-01
330.4	1.52E+18	6.00E-01
326.2	1.54E+18	4.02E-01
321.0	1.57E+18	2.61E-01
317.6	1.58E+18	1.86E-01
314.0	1.60E+18	1.29E-01
310.4	1.62E+18	9.53E-02
305.9	1.64E+18	5.99E-02
300.9	1.67E+18	3.85E-02
295.3	1.70E+18	2.39E-02
290.8	1.73E+18	1.68E-02
339.4	1.47E+18	1.27E+00
335.6	1.48E+18	8.41E-01
331.1	1.50E+18	5.83E-01
327.2	1.52E+18	4.27E-01
322.0	1.55E+18	2.56E-01
318.7	1.56E+18	1.77E-01
314.9	1.58E+18	1.27E-01
311.1	1.60E+18	8.46E-02
306.6	1.62E+18	5.46E-02
302.2	1.65E+18	3.58E-02
297.7	1.67E+18	2.15E-02
345.0	1.40E+18	2.20E+00
340.8	1.42E+18	1.58E+00
337.2	1.43E+18	1.14E+00
331.1	1.46E+18	6.60E-01
327.7	1.48E+18	5.04E-01
322.4	1.50E+18	3.02E-01
316.3	1.53E+18	1.63E-01
312.4	1.55E+18	1.06E-01
317.4	1.52E+18	1.84E-01
322.7	1.50E+18	3.16E-01
327.4	1.48E+18	4.90E-01
332.5	1.45E+18	7.60E-01
336.4	1.43E+18	1.32E+00
343.4	1.41E+18	1.89E+00
346.9	1.39E+18	2.50E+00
342.0	1.41E+18	1.77E+00
337.2	1.43E+18	1.17E+00
332.8	1.45E+18	7.70E-01
328.8	1.47E+18	5.42E-01
325.3	1.49E+18	3.79E-01
320.5	1.51E+18	2.38E-01
316.4	1.53E+18	1.51E-01
347.2	1.39E+18	2.17E+00
342.0	1.41E+18	1.47E+00
338.1	1.43E+18	1.20E+00
333.6	1.45E+18	7.67E-01
328.4	1.47E+18	4.65E-01
325.3	1.49E+18	3.44E-01
321.7	1.50E+18	2.49E-01
318.6	1.52E+18	1.77E-01
330.2	2.20E+18	5.57E-01
325.5	2.23E+18	3.96E-01
321.4	2.26E+18	2.55E-01
316.7	2.29E+18	1.50E-01
312.8	2.32E+18	1.04E-01
307.2	2.36E+18	5.03E-02
303.0	2.39E+18	3.19E-02
298.4	2.43E+18	1.62E-02
303.9	2.39E+18	4.61E-02
308.5	2.35E+18	7.46E-02
313.7	2.31E+18	1.37E-01
318.3	2.28E+18	2.21E-01
322.6	2.25E+18	3.33E-01
326.8	2.22E+18	5.23E-01
330.5	2.19E+18	7.66E-01
334.2	2.17E+18	1.07E+00
338.3	2.14E+18	1.52E+00
342.4	2.12E+18	2.06E+00
343.0	2.11E+18	2.15E+00
337.8	2.15E+18	1.48E+00
334.4	2.17E+18	1.12E+00
329.8	2.20E+18	7.20E-01
325.8	2.23E+18	4.96E-01
323.0	2.25E+18	3.84E-01
318.5	2.28E+18	2.55E-01
315.6	2.30E+18	1.90E-01
310.2	2.34E+18	1.10E-01
341.3	2.13E+18	1.88E+00
337.8	2.15E+18	1.46E+00
333.8	2.17E+18	1.06E+00
330.2	2.20E+18	7.63E-01
326.7	2.22E+18	5.72E-01
323.8	2.24E+18	4.42E-01
318.6	2.28E+18	2.91E-01
314.0	2.31E+18	2.04E-01
309.6	2.34E+18	1.29E-01
299.8	2.42E+18	4.97E-02
304.9	2.38E+18	4.17E-02
308.7	2.35E+18	6.89E-02
313.4	2.31E+18	1.21E-01
317.4	2.29E+18	1.91E-01
322.0	2.25E+18	3.47E-01
325.4	2.23E+18	5.18E-01
303.0	2.39E+18	2.82E-02
307.5	2.36E+18	6.30E-02
311.5	2.33E+18	9.54E-02
316.0	2.30E+18	1.60E-01
319.4	2.27E+18	2.46E-01
323.8	2.24E+18	4.16E-01
327.2	2.22E+18	5.25E-01
298.7	3.24E+18	2.32E-02
303.5	3.19E+18	4.28E-02
307.0	3.15E+18	6.15E-02
311.4	3.11E+18	1.07E-01
315.5	3.07E+18	1.72E-01
319.2	3.03E+18	2.62E-01
322.7	3.00E+18	3.72E-01
326.6	2.96E+18	5.68E-01
329.6	2.93E+18	8.11E-01
313.0	3.09E+18	1.34E-01
318.2	3.04E+18	2.38E-01
321.4	3.01E+18	3.32E-01
325.7	2.97E+18	5.19E-01
330.3	2.93E+18	7.98E-01
333.9	2.90E+18	1.12E+00
337.7	2.86E+18	1.55E+00
321.1	3.07E+18	3.62E-01
317.9	3.10E+18	2.65E-01
312.5	3.16E+18	1.51E-01
308.3	3.20E+18	9.60E-02
305.2	3.23E+18	6.66E-02
301.0	3.28E+18	3.69E-02
306.2	3.16E+18	5.62E-02
310.3	3.12E+18	8.74E-02
314.8	3.07E+18	1.50E-01
319.3	3.03E+18	2.59E-01
323.9	2.99E+18	4.12E-01
328.0	2.95E+18	6.33E-01
333.6	2.90E+18	1.05E+00
336.4	2.87E+18	1.38E+00
336.9	2.87E+18	1.55E+00
331.0	2.92E+18	9.25E-01
326.7	2.96E+18	7.00E-01
321.9	3.00E+18	3.66E-01
317.8	3.04E+18	2.59E-01
309.7	3.12E+18	1.25E-01
303.7	3.18E+18	6.35E-02
298.7	3.24E+18	3.53E-02
300.8	3.22E+18	4.32E-02
305.0	3.17E+18	6.34E-02
308.8	3.13E+18	9.20E-02
312.7	3.09E+18	1.38E-01
318.3	3.04E+18	2.55E-01
321.8	3.01E+18	3.58E-01
326.0	2.97E+18	5.66E-01
330.0	2.93E+18	8.56E-01
333.5	2.90E+18	1.22E+00
337.0	2.87E+18	1.62E+00
339.6	2.85E+18	2.13E+00

Cell 2

T	N_2	k_1
311.0	3.11E+18	1.21E-01
314.3	3.08E+18	1.80E-01
318.4	3.04E+18	2.66E-01
322.4	3.00E+18	3.92E-01
326.2	2.96E+18	5.56E-01
330.4	2.93E+18	8.27E-01
334.9	2.89E+18	1.31E+00
338.8	2.85E+18	1.93E+00
341.7	2.83E+18	2.51E+00
344.3	2.81E+18	3.32E+00
341.4	2.83E+18	2.26E+00
335.2	2.89E+18	1.39E+00
329.3	2.94E+18	8.02E-01
325.0	2.98E+18	5.26E-01
321.4	3.01E+18	3.80E-01
317.5	3.05E+18	2.62E-01
313.4	3.09E+18	1.77E-01
313.9	3.08E+18	1.32E-01
317.8	3.04E+18	2.07E-01
322.3	3.00E+18	3.50E-01
327.1	2.96E+18	5.77E-01
330.6	2.93E+18	8.12E-01
333.8	2.90E+18	1.16E+00
337.2	2.87E+18	1.56E+00
340.0	2.84E+18	1.95E+00
315.9	3.06E+18	1.57E-01
320.4	3.02E+18	2.68E-01
324.8	2.98E+18	4.40E-01
331.3	2.92E+18	8.68E-01
335.0	2.89E+18	1.28E+00
338.7	2.86E+18	1.82E+00
341.7	2.83E+18	2.48E+00
344.9	2.80E+18	3.33E+00
344.4	2.81E+18	3.18E+00
340.4	2.84E+18	2.17E+00
336.0	2.88E+18	1.45E+00
331.5	2.92E+18	9.41E-01
327.2	2.96E+18	6.20E-01
323.8	2.99E+18	4.36E-01
318.2	3.04E+18	2.47E-01
314.0	3.08E+18	1.56E-01
344.4	2.81E+18	3.32E+00
338.7	2.86E+18	2.00E+00
333.3	2.90E+18	1.20E+00
328.5	2.94E+18	7.60E-01
324.1	2.98E+18	4.97E-01
319.1	3.03E+18	3.04E-01
314.9	3.07E+18	1.92E-01
311.0	3.11E+18	1.19E-01
332.5	2.91E+18	1.19E+00
327.1	2.96E+18	7.38E-01
322.0	3.00E+18	4.31E-01
317.3	3.05E+18	2.71E-01
312.9	3.09E+18	1.67E-01
309.0	3.13E+18	1.06E-01
336.2	5.95E+18	1.92E+00
331.4	6.04E+18	1.28E+00
326.6	6.13E+18	7.76E-01
322.9	6.20E+18	5.33E-01
317.8	6.30E+18	3.08E-01
314.2	6.37E+18	2.06E-01
310.6	6.45E+18	1.30E-01
338.9	5.91E+18	2.47E+00
335.9	5.96E+18	1.99E+00
332.3	6.02E+18	1.36E+00
328.7	6.09E+18	9.40E-01
324.7	6.17E+18	6.31E-01
320.7	6.24E+18	4.01E-01
316.8	6.32E+18	2.61E-01
313.8	6.38E+18	1.74E-01
310.1	6.46E+18	1.08E-01
306.1	6.54E+18	6.51E-02
335.5	5.77E+18	1.94E+00
332.2	5.82E+18	1.43E+00
329.0	5.88E+18	1.00E+00
325.9	5.94E+18	7.22E-01
322.1	6.01E+18	4.77E-01

TABLE I (*Continued*)

Cell 2

T	N_2	k_1
318.6	6.07E+18	3.19E-01
314.3	6.15E+18	1.87E-01
310.5	6.23E+18	1.13E-01
307.2	6.30E+18	7.30E-02
337.9	5.81E+18	2.29E+00
333.2	5.89E+18	1.47E+00
329.2	5.96E+18	9.65E-01
325.4	6.03E+18	6.29E-01
321.2	6.11E+18	3.90E-01
317.6	6.18E+18	2.40E-01
313.2	6.27E+18	1.25E-01
309.9	6.34E+18	6.28E-02
307.2	6.39E+18	2.93E-02
332.9	5.81E+18	1.50E+00
330.3	5.86E+18	1.20E+00
326.1	5.93E+18	7.56E-01
322.2	6.00E+18	5.27E-01
319.0	6.06E+18	3.67E-01
316.2	6.12E+18	2.58E-01
312.2	6.20E+18	1.60E-01
310.0	6.24E+18	1.20E-01
306.2	6.32E+18	7.18E-02
333.2	5.81E+18	1.66E+00
331.0	5.84E+18	1.35E+00
327.8	5.90E+18	9.51E-01
324.3	5.96E+18	6.51E-01
320.9	6.03E+18	4.69E-01
317.0	6.10E+18	2.99E-01
313.5	6.17E+18	1.99E-01
311.2	6.22E+18	1.51E-01
307.6	6.29E+18	9.60E-02
331.6	1.17E+19	1.62E+00
329.4	1.17E+19	1.30E+00
324.9	1.19E+19	8.12E-01
321.0	1.21E+19	5.33E-01
317.0	1.22E+19	3.31E-01
313.3	1.23E+19	2.14E-01
308.8	1.25E+19	1.25E-01
304.7	1.27E+19	6.98E-02
330.6	1.17E+19	1.45E+00
326.6	1.18E+19	9.84E-01
321.2	1.20E+19	5.56E-01
317.5	1.22E+19	3.84E-01
313.2	1.24E+19	2.34E-01
308.7	1.25E+19	1.35E-01
305.4	1.27E+19	8.67E-02
301.1	1.28E+19	4.47E-02
331.8	1.17E+19	1.66E+00
329.7	1.17E+19	1.35E+00
326.9	1.18E+19	1.05E+00
323.6	1.20E+19	7.19E-01
319.9	1.21E+19	4.70E-01
316.6	1.22E+19	3.27E-01
312.8	1.24E+19	2.10E-01
309.7	1.25E+19	1.44E-01
306.5	1.26E+19	9.16E-02
303.0	1.28E+19	5.80E-02
298.6	1.30E+19	3.17E-02
331.9	1.17E+19	1.86E+00
329.0	1.18E+19	1.40E+00
325.8	1.19E+19	9.54E-01
321.7	1.20E+19	5.81E-01
318.8	1.21E+19	4.12E-01
315.5	1.23E+19	2.71E-01
312.1	1.24E+19	1.85E-01
308.2	1.26E+19	1.17E-01
304.4	1.27E+19	7.16E-02
300.4	1.29E+19	4.11E-02
326.9	1.18E+19	1.08E+00
323.9	1.19E+19	7.38E-01
320.7	1.21E+19	5.45E-01
317.2	1.22E+19	3.65E-01
313.9	1.23E+19	2.39E-01
311.2	1.24E+19	1.73E-01
308.0	1.26E+19	1.17E-01
304.4	1.27E+19	7.41E-02
300.5	1.29E+19	4.15E-02
296.9	1.30E+19	2.53E-02
298.6	2.59E+19	4.70E-02
302.6	2.56E+19	7.89E-02
306.7	2.52E+19	1.27E-01
310.4	2.49E+19	2.00E-01
314.3	2.46E+19	3.21E-01
319.3	2.42E+19	5.67E-01
322.9	2.40E+19	7.94E-01
296.8	2.61E+19	4.00E-02
301.5	2.57E+19	6.94E-02
306.5	2.52E+19	1.38E-01
310.5	2.49E+19	2.15E-01
315.5	2.45E+19	3.81E-01
318.6	2.43E+19	5.70E-01
321.3	2.41E+19	7.65E-01
323.4	2.39E+19	9.37E-01
300.4	2.58E+19	5.56E-02
304.5	2.54E+19	8.98E-02
308.3	2.51E+19	1.51E-01
311.8	2.48E+19	2.35E-01
315.4	2.45E+19	3.53E-01
319.3	2.42E+19	5.53E-01
322.1	2.40E+19	7.45E-01
324.8	2.38E+19	1.05E+00
293.0	2.64E+19	2.23E-02
296.4	2.61E+19	3.51E-02
300.4	2.58E+19	5.60E-02
303.7	2.55E+19	8.47E-02
306.9	2.52E+19	1.31E-01
310.3	2.49E+19	1.93E-01
313.5	2.47E+19	2.92E-01
317.0	2.44E+19	4.40E-01
319.5	2.42E+19	5.98E-01
325.5	2.38E+19	9.94E-01
323.1	2.39E+19	7.78E-01
319.8	2.42E+19	5.46E-01
316.4	2.45E+19	3.64E-01
312.9	2.47E+19	2.35E-01
309.6	2.50E+19	1.52E-01
305.8	2.53E+19	9.32E-02
302.4	2.56E+19	5.73E-02
291.4	2.66E+19	1.79E-02
295.5	2.62E+19	2.97E-02
300.2	2.58E+19	5.71E-02
303.5	2.55E+19	8.52E-02
307.1	2.52E+19	1.31E-01
310.4	2.49E+19	1.96E-01
313.8	2.47E+19	2.89E-01
316.5	2.44E+19	3.91E-01
319.4	2.42E+19	5.56E-01

Cell 3

T	N_2	k_1
315.2	3.07E+18	1.48E-01
311.8	3.10E+18	1.04E-01
308.0	3.14E+18	6.76E-02
303.8	3.18E+18	3.79E-02
299.2	3.23E+18	1.98E-02
294.3	3.29E+18	8.26E-03
314.2	3.08E+18	1.48E-01
311.3	3.11E+18	1.03E-01
308.0	3.14E+18	7.21E-02
304.6	3.18E+18	4.80E-02
301.5	3.21E+18	3.17E-02
297.2	3.25E+18	1.65E-02
293.0	3.30E+18	9.90E-03
289.7	3.34E+18	6.50E-03
321.3	2.99E+18	2.97E-01
318.3	3.02E+18	2.22E-01
315.0	3.05E+18	1.51E-01
311.9	3.08E+18	1.10E-01
308.8	3.11E+18	7.26E-02
305.6	3.15E+18	4.78E-02
301.4	3.19E+18	2.83E-02
297.8	3.23E+18	1.75E-02
322.6	3.00E+18	3.11E-01
319.9	3.02E+18	2.27E-01
316.6	3.05E+18	1.66E-01
313.2	3.09E+18	1.13E-01
308.0	3.14E+18	6.18E-02
304.5	3.18E+18	3.91E-02
300.8	3.22E+18	1.95E-02
297.1	3.26E+18	1.36E-02
295.1	3.28E+18	1.11E-02
321.3	3.01E+18	2.91E-01
318.7	3.03E+18	2.27E-01
315.4	3.07E+18	1.59E-01
311.8	3.10E+18	1.07E-01
307.7	3.14E+18	6.15E-02
304.4	3.18E+18	4.07E-02
301.0	3.21E+18	2.58E-02
296.4	3.26E+18	1.48E-02
312.2	6.13E+18	1.42E-01
309.8	6.18E+18	1.06E-01
307.9	6.22E+18	8.45E-02
305.0	6.28E+18	5.94E-02
303.1	6.32E+18	4.68E-02
300.6	6.37E+18	3.25E-02
296.9	6.45E+18	1.86E-02
294.4	6.50E+18	1.27E-02
291.7	6.56E+18	8.12E-03
312.9	6.18E+18	1.55E-01
310.8	6.22E+18	1.18E-01
307.8	6.28E+18	8.60E-02
304.4	6.35E+18	5.71E-02
301.7	6.41E+18	4.08E-02
298.3	6.48E+18	2.50E-02
294.1	6.58E+18	1.29E-02
291.6	6.63E+18	8.60E-03
312.9	6.21E+18	1.64E-01
309.7	6.28E+18	1.10E-01
306.6	6.34E+18	7.43E-02
302.6	6.42E+18	4.54E-02
299.8	6.48E+18	3.11E-02
295.5	6.58E+18	1.68E-02
292.9	6.64E+18	1.09E-02
309.4	6.31E+18	1.06E-01
306.1	6.38E+18	6.67E-02
303.1	6.45E+18	4.57E-02
299.3	6.53E+18	2.84E-02
295.8	6.60E+18	1.80E-02
292.4	6.68E+18	1.10E-02
311.7	6.24E+18	1.43E-01
309.0	6.29E+18	1.02E-01
305.1	6.37E+18	6.19E-02
301.7	6.44E+18	4.00E-02
299.2	6.50E+18	2.77E-02
296.0	6.57E+18	1.77E-02
293.3	6.63E+18	1.10E-02
290.4	6.69E+18	7.31E-03
303.9	1.27E+19	6.66E-02
301.9	1.28E+19	5.28E-02
300.7	1.29E+19	4.54E-02
298.2	1.30E+19	3.54E-02
295.3	1.31E+19	2.40E-02
292.4	1.32E+19	1.64E-02
289.9	1.33E+19	1.02E-02
304.2	1.27E+19	8.16E-02
301.6	1.28E+19	5.18E-02
299.0	1.29E+19	3.93E-02
296.6	1.30E+19	2.79E-02
293.2	1.32E+19	1.77E-02
291.1	1.33E+19	1.29E-02
288.0	1.34E+19	7.37E-03
285.6	1.35E+19	4.95E-03
303.8	1.27E+19	6.99E-02
300.8	1.29E+19	4.67E-02
298.1	1.30E+19	3.25E-02
295.5	1.31E+19	2.37E-02
292.4	1.32E+19	1.54E-02
289.6	1.34E+19	9.96E-03
287.7	1.34E+19	8.25E-03
303.8	1.27E+19	6.83E-02
301.2	1.28E+19	5.18E-02
298.3	1.30E+19	3.54E-02
295.2	1.31E+19	2.27E-02
292.6	1.32E+19	1.56E-02
290.5	1.33E+19	1.07E-02
303.9	1.28E+19	8.29E-02
301.8	1.29E+19	6.23E-02
299.2	1.30E+19	4.66E-02
296.6	1.31E+19	3.21E-02
292.5	1.33E+19	1.76E-02
288.6	1.35E+19	9.07E-03

Variable Length Cell

T	N_2	k_1
326.8	3.02E+17	1.40E-01
326.9	3.08E+17	1.50E-01
331.3	2.85E+17	2.33E-01

TABLE I (*Continued*)

Variable Length Cell		
T	N_2	k_1
331.6	2.95E+17	2.40E-01
334.8	2.89E+17	3.40E-01
337.7	2.85E+17	5.18E-01
337.9	2.79E+17	4.32E-01
339.0	2.88E+17	5.30E-01
343.2	2.87E+17	6.90E-01
344.4	2.81E+17	7.80E-01
345.2	2.80E+17	8.45E-01
348.2	2.86E+17	1.11E+00
350.2	2.84E+17	1.07E+00
352.3	2.70E+17	1.50E+00
352.4	2.70E+17	1.45E+00
354.4	2.78E+17	1.77E+00
358.5	2.78E+17	2.52E+00
361.3	2.62E+17	3.16E+00
361.4	2.63E+17	3.26E+00
368.2	2.61E+17	5.03E+00
368.4	2.61E+17	5.40E+00
377.9	2.53E+17	1.03E+01
377.9	2.53E+17	9.95E+00
383.4	2.52E+17	1.23E+01
383.4	2.52E+17	1.34E+01
320.6	8.87E+17	1.75E-01
320.7	8.87E+17	1.94E-01
321.8	9.26E+17	1.84E-01
313.3	6.11E+18	1.97E-01
314.5	6.37E+18	2.16E-01
317.6	6.03E+18	2.92E-01
320.8	6.00E+18	3.96E-01
321.9	6.01E+18	4.90E-01
327.8	6.28E+18	7.62E-01
308.8	6.48E+18	1.16E-01
322.0	9.16E+17	2.30E-01
323.5	8.70E+17	2.52E-01
324.2	8.89E+17	2.38E-01
326.7	8.88E+17	3.62E-01
326.7	8.97E+17	3.47E-01
326.8	8.97E+17	3.21E-01
331.1	8.94E+17	5.06E-01
332.3	8.61E+17	6.12E-01
336.0	8.81E+17	7.94E-01
339.0	8.47E+17	1.00E+00
344.8	8.64E+17	1.68E+00
345.1	8.44E+17	1.66E+00
350.2	8.26E+17	2.86E+00
354.2	8.03E+17	3.70E+00
357.7	8.11E+17	4.60E+00
362.8	7.97E+17	7.42E+00
363.2	7.99E+17	7.27E+00
367.4	8.08E+17	1.02E+01
368.1	8.07E+17	1.07E+01
314.7	1.47E+18	1.46E-01
321.8	1.51E+18	2.80E-01
327.8	1.48E+18	4.60E-01
331.4	1.49E+18	6.50E-01
336.0	1.43E+18	1.04E+00
344.7	1.40E+18	2.32E+00
354.1	1.37E+18	4.72E+00
314.2	3.14E+18	1.73E-01
314.4	3.20E+18	1.46E-01
320.2	2.98E+18	2.96E-01
321.3	3.01E+18	3.70E-01
328.0	2.92E+18	5.81E-01
331.6	3.03E+18	9.21E-01
336.0	2.84E+18	1.45E+00

[a] 1.494 E+18 denotes 1.494×10^{18}.

by the use of the Schwarz inequality that $J \geq 1$.

Troe[33–35] has developed an alternative approximation. Starting with a full theory of unimolecular reactions he makes a series of approximations and finally obtains an expression for k_1 as a product of three terms,

$$k_1 = k^{\mathrm{LH}} \times F^{\mathrm{SC}} \times F^{\mathrm{WC}} , \tag{19}$$

where F^{SC} and F^{WC} are broadening factors (they decrease the rate of falloff from first- to second-order kinetics) based on strong and weak collisions, respectively. At the simplest level

$$F^{\mathrm{WC}} = 1 ,$$
$$F^{\mathrm{SC}} = F^{\mathrm{SC}}_{\mathrm{cent}} [1 + (\log k_0 \mathrm{M}/k_\infty)^2]^{-1} , \tag{20}$$

where $F^{\mathrm{SC}}_{\mathrm{cent}}$ is the broadening factor at the center of the falloff curve. This is the level of approximations we have used.

Using the nonlinear least squares program mentioned above we have fit our data to the Johnston and Troe approximations. We have used simple Arrhenius forms

$$k_0 = A_0 \exp(-E_0/RT) \tag{21}$$

and

$$k_\infty = A_\infty \exp(-E_\infty/RT) \tag{22}$$

for the temperature dependences of the low and high pressure limits, k_0 and k_∞, respectively. Data are not of sufficient quality to include T^n dependences in the high and low pressure pre-exponential factors A_{00} and A_0. The four parameters A_0, A_∞, E_0, and E_∞ are allowed to vary. In addition for the Troe form $F^{\mathrm{SC}}_{\mathrm{cent}}$ is also varied. However, in the Johnston form the minimum of the curve is too shallow to allow an accurate determination of five parameters and J is set at 6.5, the value recommended by Connell and Johnston.[13] The results of these fits and the 95% confidence limits for statistical error on the activation energies are listed in Table III.

Statistical error limits for extrapolations based on these results are obtained in the following manner. The columns of an $N\times5$ matrix (or $N\times4$ for the Johnston fit) **B** are the partial derivatives of k_1, with respect to each coefficient $\partial k_1/\partial C_i$, evaluated at a particular temperature and number density. The N rows of B are generated by evaluating these derivatives at the different temperatures and number densities of interest. One then takes the matrix product $\mathbf{Err} = \mathbf{B}\times\mathbf{VCV}\times\mathbf{B}^T$, where **VCV** is the variance–covariance matrix of the coefficients supplied by the least squares fitting routine and $\mathbf{B}^T$ is the transpose of B. The square root of the diagonal elements of **Err** are the standard deviation of statistical error for the calculated rate constants.

Figure 11 compares our results to previous measurement taken at 300 K. The squares represent the data of Mills and Johnston,[5] which were obtained in a static system containing predominantly N_2, with a small amount of NO added to scavenge the NO_3 via Eq. (3). The N_2O_5 dissociation rate was determined by monitoring the product NO_2 in absorption at 436 nm. The triangles represent the data of Johnston,[9] obtained similarly to that of Mills and Johnston. The circles represent the data of Hisatsune, Crawford, and Ogg,[11] who made similar measurements, except that the N_2O_5 dissociation rate was determined by monitoring the N_2O_5 and NO_2 number densities in absorption at 5.7 and 7.2 μm,

TABLE II. Arrhenius parameters as a function of pressure.

P (Torr)	A (s^{-1})	E (kcal/mol)
10	2.89×10^{12}	19.5±0.5
30	9.27×10^{12}	20.1±0.4
50	5.35×10^{12}	19.6±0.4
75	1.73×10^{14}	21.7±0.8
100	8.47×10^{14}	22.7±0.4
200	8.74×10^{15}	24.0±0.6
400	3.66×10^{15}	23.3±0.2
800	2.49×10^{15}	22.7±0.5

TABLE III. Estimated coefficients of the analytical expression least square fits.

Expression	A_0 cm^3/s	A_∞ s^{-1}	E_0 (kcal/mol)	E_∞ (kcal/mol)	F_{cent}^{sc} or J
Troe fit	1.15×10^{-5}	1.21×10^{17}	19.70± 0.90	25.16± 0.64	0.572± 0.080
Johnston fit	5.44×10^{-6}	1.78×10^{17}	19.18± 0.58	25.41± 0.48	6.5
Connell and Johnston data	6.1×10^{-6}	1.78×10^{17}	19.02± 0.89	24.92± 1.11	6.5

respectively. This composite data set covers over three orders of magnitude in N_2 density and fairly consistently (± 50%) yield a slow variation of k_1 with $[N_2]$.

Connell and Johnston studied the reaction in a static system monitoring the 1250 cm^{-1} line of N_2O_5.[13] Their measurements were taken in either pure reactants or in a nitrogen buffer. Using the relative decomposition efficiencies of Wilson and Johnston[10] they reported their results as a function of effective nitrogen density. They did not take any data at 300 K and, therefore, their data is not represented in Fig. 11. They have interpolated their results and found them to agree with the older data at low and intermediate pressures. However, at higher pressures their results are significantly lower then the 1950's work.

The present data encompasses a much narrower pressure range than the work done in Johnston's laboratories but cover a wider range of temperature. The present data are represented by either solid inverted triangles corresponding to the best Arrhenius fit to data whose temperature range encompasses 300 K or hollow inverted triangles which are extrapolations of data taken at higher temperatures. The dashed and solid lines correspond to the Johnston and Troe fits to the data, respectively. Error bars are 95% confidence limits to statistical error for the Troe form.

The present values of the rate constants differ from the 1950's work by approximately 40% at low and intermediate pressures with much larger differences at higher pressures. Similar comparisons with Connell and Johnston's data at other temperatures show falloff curves having essentially the same curvature as ours although the present results are approximately 40% lower.

Wieder and Marcus[20] calculated the falloff curve for the case of N_2O_5 at 300 K. The curvature they predicted is quite close to that predicted here by both fits to the data. Moreover, Golden, and Baldwin have used their Gorin-type hindered rotational model[21] to calculate falloff curves. The shape of their curves agree with that predicted here and with Connell and Johnston's data.

Subtracting the reaction enthalpy of 22.2 kcal/mol (Graham and Johnston[36]) from the high pressure activation energy of 25.2 kcal/mol (average of the three values in Table III) one obtains an activation energy of 3.0 kcal/mol for the recombination reaction of NO_2 and NO_3 (Reaction 1), a surprisingly large activation energy for a simple recombination reaction such as this. Graham and Johnston also reported an activation energy at 300 K of 2.44± 0.2 kcal/mol for the reaction

$$NO_2 + NO_3 \rightarrow NO + NO_2 + O_2 \ . \qquad (23)$$

It is expected that this binary chemical reaction between NO_2 and NO_3 has a larger activation energy than the recombination reaction between them, implying a possible error in one of these activation energies.

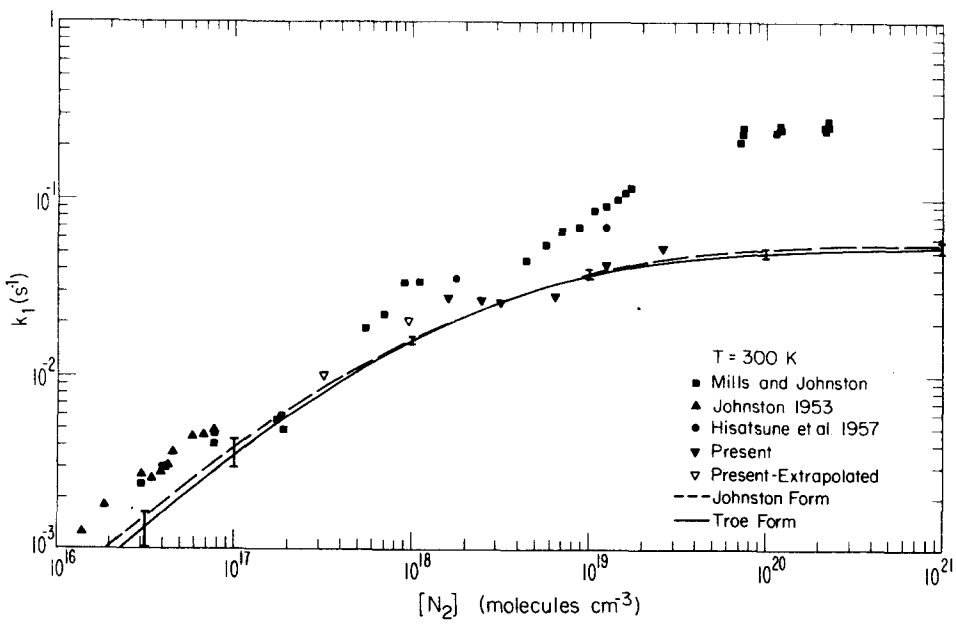

FIG. 11. Observed and calculated rate constants for the collisional dissociation of N_2O_5 by N_2 at 300 K. The measurements are those of Mills and Johnston,[5] Johnston,[9] Hisatsune *et al.*,[11] and the present data extrapolated or interpolated to 300 K. The calculations are the best fits of the present work for the Troe and Johnston approximations. Error bars are 95% confidence limits for statistical error for the Troe form.

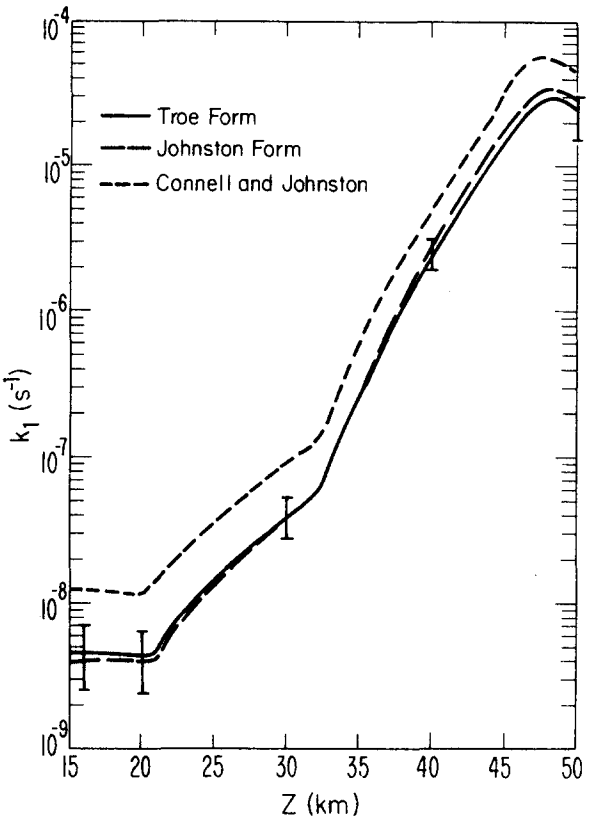

FIG. 12. Calculated rate constants for the collisional dissociation of N_2O_5 vs altitude in the stratosphere. The parameters are those taken from U. S. Standard Atmosphere, 1976.[37] Error bars are 95% confidence limits for statistical error for the Troe form.

Using the fits to the present data set, extrapolations were made to standard stratospheric conditions.[37] In Fig. 12 these extrapolations are compared to an extrapolation based on Connell and Johnston's data. The solid line, large dashed line, and small dashed line correspond to the Troe fit, the Johnston fit, and Connell and Johnston's data, respectfully. Error bars are 95% confidence limit on statistical error only for the Troe form. Throughout the entire range of stratospheric conditions no difference is evident between the two fits to the present data. The extrapolation based on Connell and Johnston's data are consistantly a factor of 2 higher than the present results. This difference corresponds to a 4° difference in temperature.

Realistically a proper extrapolation to stratospheric conditions would include a T^{-n} dependence in the low pressure pre-exponential factor. However, the data is not of sufficient quality to determine this dependence. This is usually the case in unimolecular decompositions.

SUMMARY

The flowing afterglow has been used in a novel way as a chemical ionization mass spectrometer. Using the reaction of I^- with N_2O_5 the flowing afterglow was used as a detector to study the thermal decomposition rate of N_2O_5 as a function of temperature and pressure in a nitrogen buffer. The data obtained was fit to two analytical expressions for use in atmospheric models. Comparing the results with other work we find that the pressure and temperature dependences of the present results agree quite well with those of Connell and Johnston. However, the magnitude of the rate constants differs. No explanation is given for this discrepancy. The shape of the falloff curves bring experimental results in better agreement with unimolecular reaction theory.

[1]P. J. Crutzen, I. S. A. Isaksen, and J. R. McAfee, J. Geophys. Res. **83**, 345 (1978).
[2]Shaw Liu (private communication).
[3]R. A. Ogg, Jr., J. Chem. Phys. **15**, 337, 613 (1947).
[4]J. H. Smith and F. Daniels, J. Am. Chem. Soc. **69**, 1735 (1947).
[5]R. L. Mills and H. S. Johnston, J. Am. Chem. Soc. **73**, 938 (1951).
[6]R. L. Mills, Doctoral thesis, Stanford University (University Microfilms, Ann Arbor, 1951).
[7]H. S. Johnston and R. L. Perrine, J. Am. Chem. Soc. **73**, 4782 (1951).
[8]A. R. Amell and F. Daniels, J. Am. Chem. Soc. **74**, 6209 (1952).
[9]H. S. Johnston, J. Am. Chem. Soc. **75**, 1567 (1953).
[10]D. J. Wilson and H. S. Johnston, J. Am. Chem. Soc. **75**, 5763 (1953).
[11]I. C. Hisatsune, B. Crawford, and R. A. Ogg, J. Am. Chem. Soc. **79**, 4648 (1957).
[12]G. Schott and N. Davidson, J. Am. Chem. Soc. 80, 1841 (1958).
[13]P. Connell and H. S. Johnston, Geophys. Res. Lett. 6, 553 (1979).
[14]P. Connell, Doctoral thesis, University of California, Berkeley (Lawrence Berkeley Laboratory, no. 9034, 1979).
[15]H. S. Johnston, J. Chem. Phys. 20, 1103 (1952).
[16]H. S. Johnston and J. R. White, J. Chem. Phys. 22, 1969 (1954).
[17]R. E. Powell, J. Chem. Phys. 30, 724 (1959).
[18]E. K. Gill and K. J. Laidler, Proc. R. Soc. A 250, 121 (1959).
[19]E. Thiele and D. J. Wilson, J. Chem. Phys. 35, 1256 (1961).
[20]C. M. Wieder and R. A. Marcus, J. Chem. Phys. 37, 1835 (1962).
[21]D. M. Golden and A. C. Baldwin (private communication, 1979).
[22]J. A. Davidson, A. A. Viggiano, C. J. Howard, I. Dotan, F. C. Fehsenfeld, D. L. Albritton, and E. E. Ferguson, J. Chem. Phys. 68, 2085 (1978).
[23]M. S. Zahniser (private communication, 1979).
[24]E. D. Morris and H. Niki, J. Phys. Chem. 77, 1929 (1973).
[25]F. C. Fehsenfeld and E. E. Ferguson, Planet. Space Sci. 16, 701 (1968).
[26]F. C. Fehsenfeld, C. J. Howard, and A. L. Schmeltekopf, J. Chem. Phys. 63, 2835 (1975).
[27]E. E. Ferguson, F. C. Fehsenfeld, and A. L. Schmeltekopf, Adv. At. Mol. Phys. 5, 1 (1969).
[28]A. A. Viggiano, Doctoral thesis, University of Colorado, Boulder (1980).
[29]S. Dushman and J. M. Lafferty, *Vacuum Techniques* (Wiley, New York, 1966), pp. 80–87.
[30]H. S. Johnston, J. Am. Chem. Soc. 73, 4542 (1951).
[31]P. V. Tryon and J. R. Donaldson, *Statlib Manual* (NBS Center for Applied Mathematics, Boulder, 1978).
[32]C. N. Hinshelwood, *The Kinetics of Chemical Change* (Oxford University, Oxford, 1940).

[33]J. Troe, J. Phys. Chem. 83, 114 (1979).
[34]J. Troe, ***Physical Chemistry Series Two, Chemical Kinetics***, edited by D. R. Herschbach (Butterworths, London, 1976), Vol. 9, pp. 1–24.
[35]J. Troe, Physical Chemistry: ***An Advanced Treatise. V. VIB, Kinetics of Gas Reactions***, edited by H. Eyring, D. Henderson, and W. Jost (Academic, New York, 1975), pp. 835–929.
[36]R. A. Graham and H. S. Johnston, J. Phys. Chem. 82, 254 (1978).
[37]U. S. Standard Atmosphere (1976), U. S. Printing Office, Washington, D.C. 20402, stock no. 003-017-00323-0.